Li *et al. Energy Mater.* **2025**, *5*, 500036
DOI: 10.20517/energymater.2024.127

Energy Materials

Article

Open Access

Stable hexaazatrinaphthylene-based covalent organic framework as high-capacity electrodes for aqueous hybrid supercapacitors

Xu Li[1,2], Zhenhu Li[1,3,*], Yulin Zhang[1,3], Hanlin Guo[4], Meiying Zou[1,3], Haoxiang Li[1,3], Yuping Liu[1,3], Shuangyi Liu[1,3,*]

[1]Research Center for Electrochemical Energy Storage Technologies, Chongqing Institute of Green and Intelligent Technology, Chinese Academy of Sciences, Chongqing 400714, China.
[2]Chongqing CAS Supercap Technology Co., Ltd., Chongqing 401329, China.
[3]Chongqing School, University of Chinese Academy of Sciences, Chongqing 400714, China.
[4]School of Physics and Electronic Engineering, Harbin Normal University, Harbin 150025, Heilongjiang, China.

[*]**Correspondence to:** Dr. Zhenhu Li and Prof. Shuangyi Liu, Research Center for Electrochemical Energy Storage Technologies, Chongqing Institute of Green and Intelligent Technology, Chinese Academy of Sciences, 266 Fangzheng Avenue, Chongqing 400714, China. E-mail: lizhenhu@cigit.ac.cn; liushuangyi@cigit.ac.cn

How to cite this article: Li, X.; Li, Z.; Zhang, Y.; Guo, H.; Zou, M.; Li, H.; Liu, Y.; Liu, S. Stable hexaazatrinaphthylene-based covalent organic framework as high-capacity electrodes for aqueous hybrid supercapacitors. *Energy Mater.* **2025**, *5*, 500036. https://dx.doi.org/10.20517/energymater.2024.127

Received: 19 Aug 2024 **First Decision:** 4 Nov 2024 **Revised:** 1 Dec 2024 **Accepted:** 9 Dec 2024 **Published:** 23 Jan 2025

Academic Editors: Hao Liu, Liming Jin **Copy Editor:** Ping Zhang **Production Editor:** Ping Zhang

Abstract

Covalent organic frameworks (COFs) have great potential as electrodes for aqueous hybrid supercapacitors (AHCs) owing to their designable structure and resourceful advantages. However, their low capacities and high structure instability in aqueous electrolytes limit the onward practical applications. Here, we have synthesized robust hexaazatrinaphthylene-based COF (HATN-COF) by a simple condensation between cyclohexanehexone and 2,3,6,7,10,11-hexaiminotriphenylene. The π-conjugation skeleton, porous structure, and high-proportioned imine bonds give HATN-COF sufficient electron and ion diffusion pathways for rapid reaction kinetics together with abundant exposed active sites for large capacity. Meanwhile, the formed hydrogen bond networks by ethanol molecules in frameworks improve the acid-base tolerance. As a consequence, HATN-COF delivers an exceptional specific capacity of 367 $mAhg^{-1}$ at 1 A g^{-1} (maximum value among reported COF-related electrodes in AHCs), high rate capability with 259.7 $mAhg^{-1}$ at 20 A g^{-1}, and superior cycle durability with retaining 97.8% of its capacity even after 20,000 cycles. Moreover, the AHC, constructed by HATN-COF as the positive electrode and activated carbon as the negative electrode, exhibits a large energy density of 67 Wh kg^{-1} at a power density of 375 W kg^{-1}, accompanied by outstanding cycling stability. The research presents a promising approach for designing

high-performance COF electrodes for advanced AHCs.

Keywords: Covalent organic framework, hexaazatrinaphthylene, electrode materials, aqueous hybrid supercapacitor

INTRODUCTION

Aqueous hybrid supercapacitors (AHCs) consist of a battery-like electrode, a capacitive electrode, and an aqueous electrolyte. They are competitive electrochemical energy storage devices for large-scale applications due to their merits of the potential coexistence for delivering high energy density, exceptional power density, excellent cyclability and good safety[1-5]. Various inorganic battery-type electrode materials[6], in particular, transition metal oxides[7], transition metal sulfides[8] and transition metal hydroxides[9], have been extensively employed as high-capacity cathodes in AHCs[10,11]. For example, $Zn_{0.5}Cu_{0.5}Co_2O_4$ with oxygen vacancies[12] exhibits a specific capacity of 271 mA h g^{-1} at 1 A g^{-1}. $NiCo_2S_4$ decorated in mesoporous carbon hydrogel[13] shows a high specific capacity of 317.9 mAh g^{-1} at 1 A g^{-1}. Mesoporous $Ni(OH)_2$ cubic nanocages intercalated with VO_4^{3-}[14] obtain a specific capacity of 280 mAh g^{-1} (approaching the theoretical value) at 1 A g^{-1}. However, these traditional metal-based (Ni, Co, and Cu) cathode materials face limited transition metal element resources and inferior cycle performance due to their large structural changes upon repeated charge-discharge processes. By contrast, organic compounds linked by covalent bonds primarily comprise abundant elements such as C, H, O, N, and S. These compounds exhibit characteristics of resource sustainability, adjustable molecular constitution and flexible structure, making them suitable for sustainable application of AHCs[15].

As a typical class of crystalline porous organic compounds, covalent organic frameworks (COFs) have garnered attention as promising electrode material candidates due to their abundant redox-active groups and periodic networks with highly cross-linked organic molecules[16,17]. They also show unique physicochemical properties, including high crystallinity, porous structure and high surface area, which could be beneficial for electrolyte ion diffusion. In particular, π-conjugated imine (C=N)-based COFs, such as e-COF[17], 4-(Dicyanomethylene)-2,6-dimethyl-4*H*-pyran (DDP)-based covalent triazine frameworks (CTFs)[18], covalent organic framework-5 (COF-5)[19] and hexamine dipyrazinoquinoxaline-based covalent organic framework (HADQ COF)[20], have obtained remarkable success as electrode materials for both nonaqueous and aqueous batteries, as well as supercapacitors thanks to the structural benefits of rich redox centers and intrinsic electrical conductivity. Despite possessing a high theoretical capacity, imine-based COFs suffer from infertile redox active sites and poor structure stability, especially in aqueous acidic or alkaline electrolytes.

So far, only a few imine-linked COFs have been reported as supercapacitor electrodes in aqueous media. For example, a hexaazatrinaphthylene (HATN)-based COF containing an aza-fused π-conjugated framework displays a small surface area and hence a general specific capacitance of 663 F g^{-1} at 1 A g^{-1}, while its retaining stability through 7,500 cycles test in 1 M H_2SO_4[21]. A porphyrin-based COF linked by imine bonds shows an extensive surface area accompanied by an impressive specific capacitance of 1,443 F g^{-1} at 1 A g^{-1} but relatively short 3,000 cycles when tested in 0.5 M H_2SO_4 electrolyte[22]. In this case, the π-conjugated HATN-based COFs could comparatively stabilize imine linkages in rigid aromatic frameworks while compromising the redox activity in acidic electrolytes[23,24]. On the other hand, few publications have reported imine-based COFs for alkaline AHCs, showing ordinary specific capacitances (< 800 F g^{-1} at 1 A g^{-1})[25,26]. Comprehensively speaking, the specific capacities demonstrated by COF electrodes are still lower than those of metal-based electrodes for AHCs on account of the existence of unusable active groups.

Therefore, it is challenging to design stable and highly porous imine-based COFs with high-efficiency utilization of active sites for AHCs with competitive performance.

In the present study, we report a stable imine-linked HATN-COF with abundant pore structure as high capacity and long lifetime AHC organic electrodes, synthesized via a one-step solvothermal condensation process through reacting cyclohexanehexone and 2,3,6,7,10,11-hexaiminotriphenylene (HAT) in an ethanol solvent. The high crystalline and porous structures of π-conjugated HATN-COF not only facilitate electron and ion transport but also ensure a broader exposure of functional active sites conducive to faradaic reactions. Simultaneously, incorporating the ethanol molecules in frameworks, the HATN-COF presents high chemical stability in strong acids and bases because of the formation of hydrogen bond networks by ethanol molecules that can protect the imine bonds. Consequently, HATN-COF shows a remarkably large specific capacity (367 $mAhg^{-1}$ at 1 A g^{-1}) in alkaline conditions, exceeding the current state-of-the-art COF-based positive electrodes, while maintaining favorable rate performance and long-term cycling stability. Furthermore, an AHC assembled with HATN-COF and activated carbon (AC) as positive and negative electrodes, respectively, demonstrates superior energy density, high power density and remarkable cycling durability, thereby demonstrating its high potential as an organic electrode for future AHCs.

EXPERIMENTAL

Synthesis of HATN-COF

The synthesis of HATN-COF was achieved through a modified method[27]. A solution of hexaketocyclohexane (HKH) octahydrate (89.6 mg, 0.287 mmol) and 2,3,6,7,10,11-hexaaminotriphenylene hexahydrochloride (314 mg, 0.988 mmol) was mixed in 36 mL ethanol using a round-bottom flask. To this mixture, 4 mL about 36% concentrated hydrochloric acid was cautiously added. The resulting solution was then heated under reflux at 160 °C for 72 h in a sealed flask, resulting in the formation of a brown suspension containing the desired product. After cooling to room temperature, the products were isolated via centrifugation, washed repeatedly with ethanol, and dried under vacuum at 60 °C for 24 h in a 79% yield.

Physical characterization

The carbon framework of HATN-COF was analyzed using ^{13}C solid-state nuclear magnetic resonance (SSNMR) on a Bruker 400 MHz spectrometer. Morphological and structural features were investigated through transmission electron microscopy (TEM, Philips Tecnai 20) and scanning electron microscopy (SEM, JSM-7800F, 10 kV) coupled with energy-dispersive X-ray spectroscopy (EDS). Powder X-ray diffraction (XRD, Rigaku Dmax-2000) and high-resolution transmission electron microscopy (HRTEM) were employed to characterize the crystal structures. Functional groups were identified via Fourier transform infrared (FTIR) spectroscopy (Agilent Cary 630) in the 1,000-4,000 cm^{-1} range using KBr pellets. Chemical composition and valence states were further explored using X-ray photoelectron spectroscopy (XPS, Thermo Scientific K-Alpha). Raman spectroscopy (Renishaw InVia) at 532 nm was conducted for vibrational mode analysis, calibrated using a silicon wafer peak at 520 cm^{-1}. The spectra were collected between 200 cm^{-1} and 3,200 cm^{-1}, with the sample exposed to the air under ambient conditions. The measurements were obtained with an acquisition time of 30 s and 1 accumulation. Elemental analysis for C and N was performed on a vario EL cube analyzer. Thermogravimetric analysis (TGA) was performed using a TGA/differential scanning calorimetry (DSC) I thermal analyzer under a N_2 atmosphere with the temperature elevated from room temperature to 1,000 °C at a constant heating rate of 5 °C min^{-1}. Optical properties were assessed through diffuse reflectance spectroscopy at room temperature using an ultraviolet-visible spectrophotometer (UV-Vis) (UV-Vis, UV-3101PC, Shimadzu).

Electrochemical measurements

For electrochemical testing, the working electrode was prepared by blending the active material, acetylene black, and polyvinylidene fluoride (PVDF) in an 8:1:1 mass ratio in N-methyl-2-pyrrolidone to form a homogeneous paste. This paste was subsequently coated onto a Ni foam substrate (1 cm × 1 cm) and dried under vacuum at 85 °C for 12 h. The mass of active material loaded per electrode was precisely controlled at approximately 3 mg using a microbalance (Sartorius, QUINTIX35-1CN) with 0.01 mg accuracy. Electrochemical measurements were conducted in both three- and two-electrode configurations using 6 mol L^{-1} KOH as the electrolyte.

In the three-electrode setup, the Ni foam electrode, platinum foil and Hg/HgO electrode were used as the working, counter and reference electrodes, respectively. The specific capacity (Qs, mAh g^{-1}) was calculated from galvanostatic charge-discharge (GCD) curves using[28]

$$Qs = I\Delta t/3.6m \quad (1)$$

where I is the discharge current, Δt is the discharging time, and m is the mass of the active material.

Cyclic voltammograms (CV), GCD and cycle life were performed on a CHI 760E workstation and Neware battery test system at ambient temperature. Electrochemical impedance spectroscopy (EIS, 100 kHz^{-1} Hz) was achieved at the open circuit with 5 mV amplitude on CHI 760E workstation.

For the two-electrode system, HATN-COF and AC were used as positive and negative electrodes, respectively. The charge (Q) balance between positive and negative electrodes is maintained according to the relationship

$$m_+/m_- = C_- \times \Delta V_-/C_+ \times \Delta V_+ \quad (2)$$

where C is the specific capacity, and V is the potential window, respectively.

All electrochemical measurements of the two-electrode system were performed on a CHI 760E electrochemical working station. The cycle stability test was conducted on the Neware battery tester. Energy density (E) and power density (P) of AHC were evaluated using[29]

$$E = C \times (\Delta V)^2/7.2 \quad (3)$$

$$P = E \times 3600/\Delta t \quad (4)$$

where ΔV, C and Δt are the voltage window (V), specific capacitance (F g^{-1}), and discharge time (s) in two electrodes, respectively.

RESULT AND DISCUSSION

As illustrated in the schematic diagram of Figure 1A, the synthesis of HATN-COF ($C_{20}H_{12}N_6$) involves a solvothermal condensation reaction between HKH and HAT in an acidic ethanol solution. Powder X-ray Diffraction (PXRD) analysis is initially collected to identify the structure and crystallinity of HATN-COF [Figure 1B]. Two sharp 2θ peaks at 7.3° and 26.3° correspond to (100) and (001) facets of HATN-COF, respectively, representing high crystallinity. This experimental pattern shows a good match with the

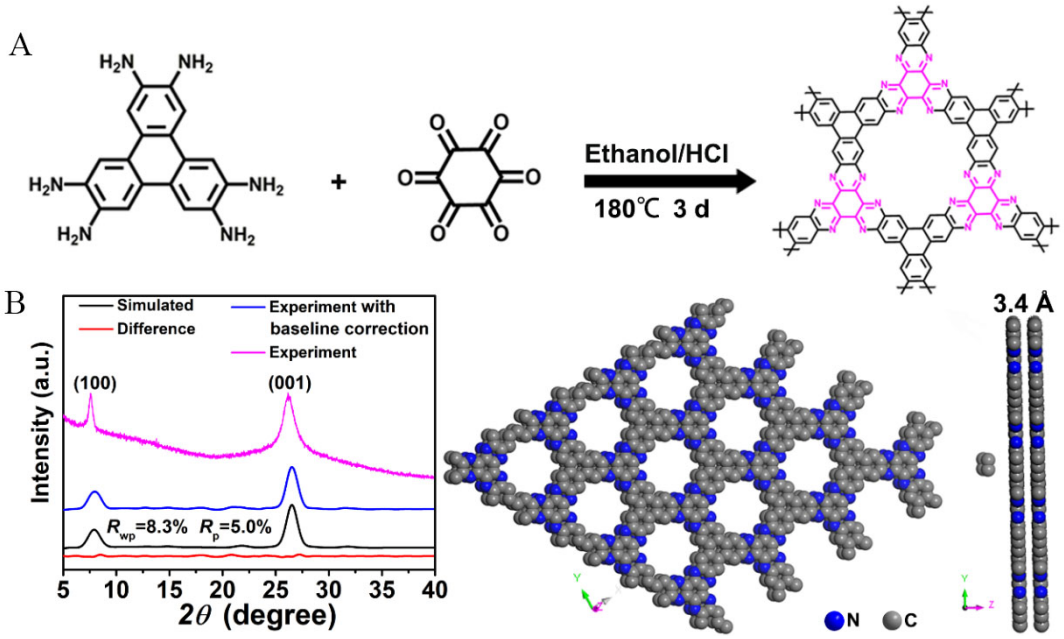

Figure 1. Synthesis and structural characterization of HATN-COF. (A) Synthetic scheme; (B) The experimental and simulated XRD patterns and corresponding space-filling model. HATN: Hexaazatrinaphthylene; COF: Covalent organic frameworks; XRD: X-ray diffraction.

simulated PXRD pattern of the AA-stacking structure by Materials Studio[30], which has low residuals (R_p = 5.0% and R_{wp} = 8.3%). Specially, the peak at 7.3° corresponds to the periodic pore structure with a pore width of 11.6 Å, in good concordance with the simulated pore diameter of HATN-COF [Supplementary Figure 1], facilitating the efficient transfer of electrolyte ions within the electrode material to ensure the rapid reaction kinetics. Meanwhile, the broad peak at 26.3° is mainly ascribed to the extended π-conjugated laminated construction with an interlayer spacing of 3.4 Å and π-π stacking between the HATN-COF layers corresponds to the (001) plane[31,32].

SEM connected with EDS analysis and TEM techniques have been employed to gain further insight into microstructure and constituent of HATN-COF. A SEM image shows uniform microrod morphology featuring a length dimension approximating 2 μm × 200 nm [Figure 2A]. EDS elemental mapping images depict uniformly distributed C and N elements over the entire HATN-COF rod [Figure 2B and Supplementary Figure 2]. Furthermore, elemental analysis displays a C/N atomic ratio of 3.4, approaching the theoretical ratio of 3.3 [Supplementary Table 1], confirming the elemental composition of the HATN-COF. A TEM image manifests the rods consist of layered stacking [Figure 2C]. It is further confirmed by ultrasonic crushing of the HATN-COF powder in ethanol, where the multilayered stacking structure is more obviously visible in the SEM and TEM images [Supplementary Figures 3 and 4], ascribable to the robust interlayer π-π stacking interaction among neighboring layers of conjugated aromatic rings[33]. Additionally, the Selected Area Electron Diffraction (SAED) pattern [Figure 2C] unveils two typical (100) and (001) crystalline facets of the HATN-COF crystal phase. These findings are in excellent agreement with the PXRD pattern. ^{13}C SSNMR analysis further demonstrates the carbon skeleton of HATN-COF structure. The ^{13}C SSNMR spectrum exhibits four obvious peaks at 105, 125, 140, and 150 ppm [Figure 2D], which are characteristic of the carbon signals of C-C, C=C, C-N and C=N in HATN-COF framework[34]. The FTIR spectrum also identifies interrelated functional moieties within HATN-COF [Figure 2E]. The peaks at 1,646 and 1,432 cm^{-1} are ascribed to the stretch vibrations of C=N[35] and C-N[36], respectively, signifying the

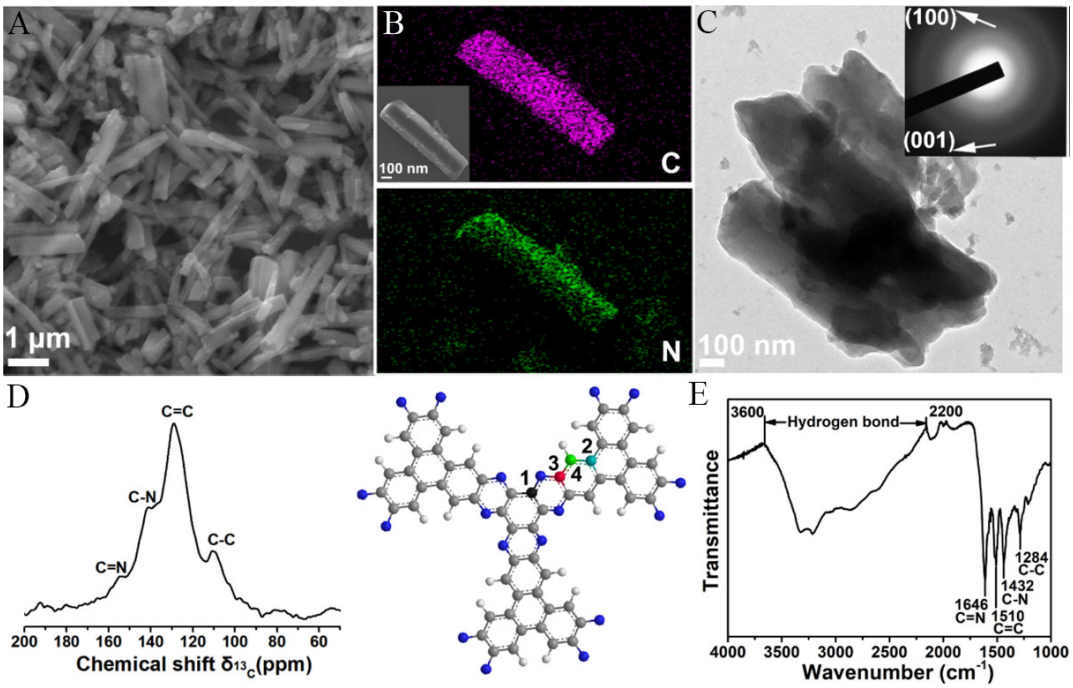

Figure 2. Characterizations of HATN-COF. (A) SEM image; (B) EDS elemental mappings; (C) TEM image (inset, SAED image); (D) ^{13}C SNMR spectrum and (E) FTIR spectrum. HATN: Hexaazatrinaphthylene; COF: Covalent organic frameworks; SEM: Scanning electron microscopy; EDS:Energy-dispersive X-ray spectroscopy; TEM: Transmission electron microscopy; SAED: Selected area electron diffraction; FTIR: Fourier transform infrared; SNMR: Solid-state nuclear magnetic resonance.

formation of imine linkages. Simultaneously, the peaks at 1,510 and 1,284 cm^{-1} are assigned to the stretch vibrations of C=C and C-C in HAT units, further confirming the formation of HATN polymers. Besides, the broad peak between 3,600 and 2,200 cm^{-1} corresponds to the hydrogen bonding stretch from solvent ethanol molecules[37]. This is also demonstrated by the TGA-DSC characterization, where some crystalline ethanol molecules could be present in the HATN-COF framework [Supplementary Figure 5]. The hydrogen-bonding networks have been reported to suppress the acid/base offense on nitrogen heterocycles[38,39].

XPS is conducted to verify the HATN-COF chemical constitution. The XPS survey spectra clearly display the distinctive peaks associated with C, N, and O components within the HATN-COF [Figure 3A and Supplementary Table 2][40]. Moreover, the deconvoluted peaks in the C 1s spectrum in Figure 3B, located at 284.6, 285.0, 285.5 and 284.0 eV, are attributed to the C=C[41], C-O-H, C=N[42] and C-N stemmed from triphenylene, ethanol guest molecule and formed imine, respectively. The deconvoluted peaks of N 1s at 398.7 and 400.5 eV in Figure 3C are severally assignable to C=N[35] bond and C-N-C linkage within the HATN unit[43]. Additionally, the O 1s signals observed at 531.7, 532.8 and 533.6 eV are indicative of the C-O bond[44], C=O and -OH group, respectively [Supplementary Figure 6][38], which are ascribed to the intercalated ethanol molecules in HATN-COF. UV-vis spectroscopy of HATN-COF reveals a wide absorbance ranging from 250 to 480 nm [Supplementary Figure 7], corresponding to the syncretic transition of π-π* and n-π* for HATN unit, which is a conjugated framework composed with C=C and C=N linkages[45], also evidenced by the XPS, FTIR and ^{13}C SSNMR results. Furthermore, the maximum absorption wavelength ends at 789 nm the intersection at the X-axis in Supplementary Figure 7, attributable to a small band gap of 1.6 eV, which indicates the semiconductive behavior. Besides, the Raman spectrum of HATN-COF shows two obvious tagged bands centered at 1,367 and 1,508 cm^{-1}[Figure 3D], corresponding

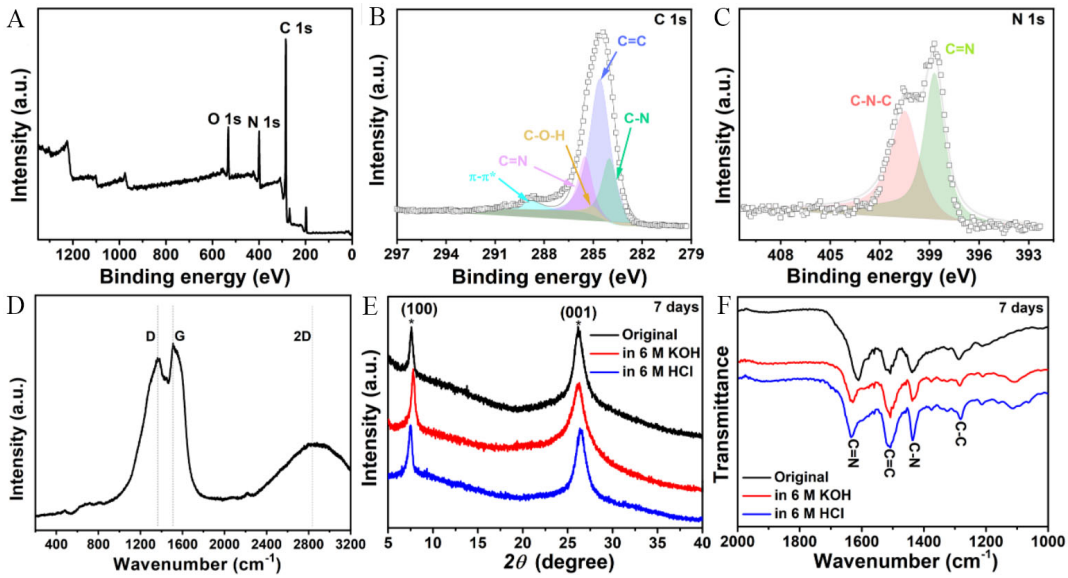

Figure 3. Characterizations and acid-alkali tolerance test of HATN-COF. XPS analysis, (A) survey spectrum and the high-resolution (B) C 1s; and (C) N 1s spectra; (D) Raman spectrum; (E) XRD patterns and (F) FTIR spectrum of HATN-COF after soaking in 6 M HCl and 6 M KOH for seven days. HATN: Hexaazatrinaphthylene; COF: Covalent organic frameworks; XPS: X-ray photoelectron spectroscopy; XRD: X-ray diffraction; FTIR: Fourier transform infrared.

to defective D band and E_{2g} mode G band[46], respectively, which is attributed to the basic features of COFs with the extended π-conjugated structure[47]. Notably, a broad peak observed at 2836 cm^{-1} is characteristic of the presence of the 2D band[40], indicating a significant level of graphitization achieved in HATN-COF[40]. The above results indicate that the HATN-COF has been successfully synthesized.

N_2 adsorption-desorption measurement further reveals the porosity of HATN-COF. Supplementary Figure 8 depicts the characteristic type-I and type-IV mixed isotherm, which demonstrates the presence of micro- and mesoporous with a specific surface area of approximately 410 m^2 g^{-1} as determined by a Brunauer-Emmett-Teller method and a pore volume of 0.28 cm^3 g^{-1} by a density functional theory method. Simultaneously, the pore size distribution (PSD) is primarily located at 6-13 Å, where a PSD of 11.6 Å agrees with the simulated structure model [Supplementary Figure 1], while the smaller pore of 6-10 Å could result from the filled ethanol molecules on some pores. The small portion of mesopores of 34-40 Å could be due to the stacking of small nanosheet structures[38]. Particularly, the chemical stability of HATN-COF is assessed by being immersed in high-concentration acidic and alkaline electrolytes. XRD patterns show the unaltered crystalline structure of HATN-COF after soaking in 6 M HCl and 6 M KOH for seven days [Figure 3E], where the position and strength of (100) and (001) facets are both retained. The unaltered C=N and C-N covalent linkages within the FTIR spectrum underscore the remarkable resilience of HATN-COF against acidic and alkaline conditions [Figure 3F], stemming from the shielding of imine linkages through hydrogen bonds that safeguard against H^+ or OH^- attacking[27,48]. Obviously, the stable HATN-COF is a potential electrode material to be used in alkaline hybrid supercapacitors.

Electrochemical performance of HATN-COF electrode material is first evaluated through a three-electrode setup, which operates within a potential range spanning 0~0.6 V in 6 M KOH electrolyte solution. As the scan rate is incremented from 5 to 100 mV s^{-1}, all cyclic voltammetry (CV) curves display a group of broad redox peaks while preserving a similar shape with escalated currents [Figure 4A], indicating a quasi-reversible reaction process derived from the redox-active imines. The relatively negligible currents in

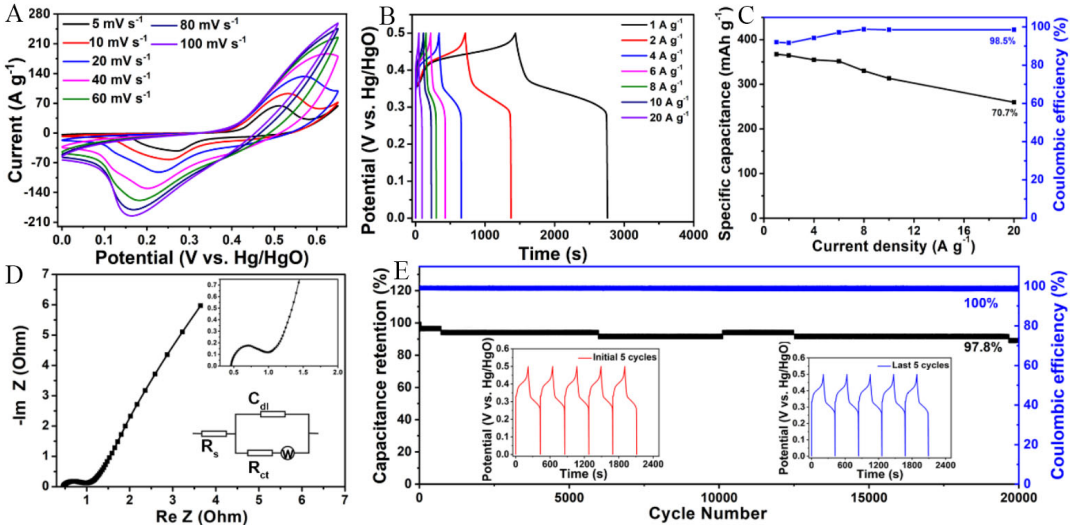

Figure 4. Electrochemical performances of HATN-COF electrode. (A) CV profiles at varying scan rates; (B) GCD profiles at various current densities; (C) Rate capability performance and coulomb efficiency; (D) Nyquist plots, an inset showing enlarged portion; (E) Cycling performance at 6 A g^{-1}. The inset provides the GCD profiles for both the initial and the final five cycles. HATN: Hexaazatrinaphthylene; COF: Covalent organic frameworks; CV: Cyclic voltammograms; GCD: Galvanostatic charge-discharge.

the neutral electrolyte further confirm the redox reaction process for HATN-COF material instead of the electrostatic adsorption [Supplementary Figure 9]. Generally, the dependency of the peak current (i) on the scan rate (v) adheres to the power law, expressed as[49]: $i=av^b$, with a and b serving as variable constants. Upon correlating log (i) versus log (v), the b values for the oxidation and reduction peaks are determined to be 0.61 and 0.57, respectively, which suggests a typical battery-type behavior [Supplementary Figure 10]. Subsequently, performing the GCD assessment offers a profound understanding of the charge storage abilities exhibited by the HATN-COF electrode [Figure 4B and Supplementary Table 3]. All GCD curves show symmetric platforms at various current densities, which further confirms a battery-type characteristic of HATN-COF with nice reversibility. Impressively, the HATN-COF delivers an unexpected specific capacity of 367.3 mAh g^{-1} (equivalent to 2,644.5 F g^{-1}) under 1 A g^{-1}, surpassing numerous reported COF materials [Supplementary Table 4][32], such as TaPa-Py-COF (209 F g^{-1} at 0.5 A g^{-1})[50], anthraquinone-based covalent organic frameworks/graphene composite aerogel (DAAQ-COFs/GA) (378 F g^{-1} at 1 A g^{-1})[51] and TDFP-1 (418 F g^{-1} at 0.5 A g^{-1})[52], while demonstrating comparable performance to high-capacity Ni/Co-based inorganic materials [e.g., CF@(Ni, Co)Se-2, 188 mAh g^{-1}[53]; Ni-Co-LDH-4:1, 255 mAh g^{-1}[28]; Ni_9S_8, 278 mAh g^{-1}[54]. All measures at 1 A g^{-1}]. Upon escalation of current densities to 20 A g^{-1}, the HATN-COF maintains an impressive high specific capacity of 259.7 mAh g^{-1} with 70.7% retention relative to 1 A g^{-1} [Figure 4C], showing splendid rate performance. So, the conjugated HATN-COF with abundant pores can provide enough channels for a fast redox reaction. Furthermore, the behavior of charge transfer is investigated using EIS measurements. According to the Nyquist plot in Figure 4D, the HATN-COF exhibits both small equivalent series resistance (R_s) value at 0.46 Ω in conjunction with a charge transfer resistance (R_{ct}) value at 0.57 Ω, which signifies low resistance to ionic kinetics. What is more, after enduring 20,000 cycles at 6 A g^{-1}, the HATN-COF still presents a competitively large specific capacity of 344 mAh g^{-1} (maintaining 97.8% of its original capacitance, Figure 4E), demonstrating its ultralong cycle life, which surpasses that of the most reported organic materials [Supplementary Table 4][52]. The excellent cycling performance in alkaline electrolytes could be attributed to the high alkaline tolerance for HATN-COF structure. Moreover, the HATN-COF electrode after cycling the GCD test is further characterized by utilizing SEM, XRD and FTIR [Supplementary Figure 11], where the changeless morphology, crystal, and chemical structure consistently reconfirm high electrochemical stability of HATN-COF.

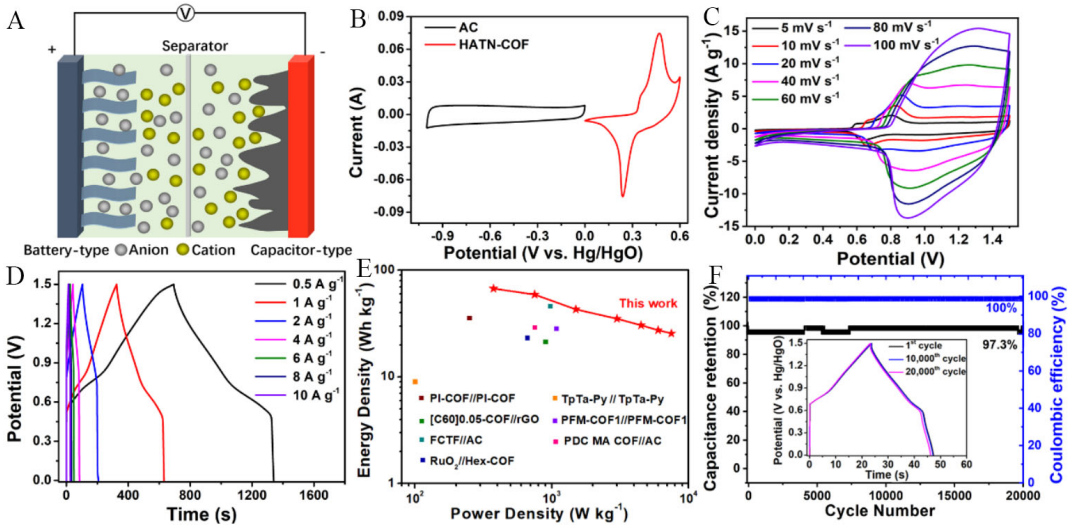

Figure 5. Electrochemical performances of HATN-COF//AC AHC. (A) Schematic illustrations of AHC construction; (B) CV curves at 10 mV s^{-1} of the HATN-COF and AC serving as positive and negative electrodes, respectively, within a three-electrode configuration utilizing 6 M KOH electrolyte; (C) CV curves of HATN-COF//AC at diverse scan rates; (D) GCD curves of HATN-COF//AC system at various current densities; (E) Ragone plots comparing the energy- and power-density of assembled device with other materials reported in literature; (F) Cycling stability performance. HATN: Hexaazatrinaphthylene; COF: Covalent organic frameworks; CV: Cyclic voltammograms; AHCs: Aqueous hybrid supercapacitors; GCD: Galvanostatic charge-discharge; AC: Activated carbon.

To further evaluate the potential of HATN-COF for practical use, an AHC is constructed using HATN-COF as the positive electrode material and AC as the negative electrode material [Figure 5A]. In contrast to HATN-COF, AC displays rectangular CV and linear GCD curves [Supplementary Figure 12], which is a distinctive feature associated with the electrochemical double-layer behavior. The specific capacity for AC is 300 F g^{-1} at 1 A g^{-1}, while retaining a respectable 240 F g^{-1} at 20 A g^{-1}. To ensure equilibrium in charge distribution between the positive electrode and negative electrode of the AHC, a specific mass ratio of HATN-COF: AC = 1:6 is employed. As shown in Figures 5B and Supplementary Figure 13, HATN-COF and AC operate within opposite potential ranges, while the cell maintains a stable voltage window of 1.5 V. Upon escalation from 5 to 100 mV s^{-1}, CV curves of HATN-COF//AC AHC exhibit a well-maintained shape, suggesting good reaction reversibility [Figure 5C]. Calculated from the GCD test [Figure 5D], at 0.5 A g^{-1}, the specific capacity of HATN-COF//AC AHC reaches a high value of 215.4 F g^{-1}. Correspondingly, the device of HATN-COF//AC AHC provides the supreme power-density with 7,500 W kg^{-1} and maximum energy density with 67.3 Wh kg^{-1} at 375 W kg^{-1}, outperforming most COF-based supercapacitors [Figure 5E and Supplementary Table 5], such as RuO_2//Hex-COF (23.3 W h kg^{-1} at 661.2 W kg^{-1})[21], FCTF//AC (46.3 W h kg^{-1} at 975 W kg^{-1})[55] and TpTa-Py//TpTa-Py (9.06 W h kg^{-1} at 100 W kg^{-1})[50]. Furthermore, at 6 A g^{-1}, the HATN-COF//AC AHC delivers a capacity retention of 97.3% after 20,000 cycles [Figures 5F and Supplementary Figure 14], surpassing most reported COF-based supercapacitors, confirming the excellent cyclic stability. In summary, the HATN-COF, with its stable porous HATN structure, serves as electrode material that enables the AHC full device to achieve superior energy storage performance.

CONCLUSION

In summary, an imine-linked HATN-COF with high acid-base endurance is successfully synthesized and applied as the electrode material in AHC. The porous structure, robust HATN skeleton and hydrogen-bonding protection make HATN-COF possess highly efficient and extremely stabilized redox-active sites. Consequently, the HATN-COF reveals a remarkably elevated specific capacity reaching

367.3 mAh g^{-1} under 1 A g^{-1}, impressive rate capability retaining 259.7 mAh g^{-1} even at 20 A g^{-1}, and displays superb cyclability retaining 97.8% retention of its initial capacity post 20,000 cycles at 6 A g^{-1}. Moreover, the HATN-COF//AC AHC device achieves an outstanding energy density of 67.3 W h kg^{-1} at 375 W kg^{-1} plus a long cycling stability of up to 20,000 cycles without obvious capacity fading. This work presents a promising method to develop strong COF electrode materials for high-performance AHCs.

DECLARATIONS

Authors' contributions

Conceptualization, formal analysis, investigation, software, resources, writing - original draft: Li, X.
Conceptualization, formal analysis, resources, supervision, writing - review and editing, funding acquisition: Li, Z
Formal analysis: Zhang, Y.
Software, formal analysis: Guo, H.
Resources: Zou, M.
Formal analysis: Li, H.
Resources: Liu, Y.
Resources, supervision, funding acquisition: Liu, S.

Availability of data and materials

All datasets generated for this study are included in the article Supplementary Materials.

Financial support and sponsorship

This work was supported by the Youth Innovation Promotion Association of the Chinese Academy of Sciences (2020380) and the self-deployment research project of the Chongqing Institute of Green and Intelligent Technology (2023000183).

Conflicts of interest

All authors declared that there are no conflicts of interest.

Ethical approval and consent to participate

Not applicable.

Consent for publication

Not applicable.

REFERENCES

1. Yang, E.; Shi, X.; Wu, L.; et al. A low-cost moderate-concentration hybrid electrolyte of introducing $CaCl_2$ and ethylene glycerol enables low-temperature and high-voltage micro-supercapacitors. *Adv. Funct. Mater.* **2024**, *34*, 2313395. DOI
2. Nan, J.; Sun, Y.; Yang, F.; et al. Coupling of adhesion and anti-freezing properties in hydrogel electrolytes for low-temperature aqueous-based hybrid capacitors. *Nano-Micro. Lett.* **2023**, *16*, 22. DOI PubMed PMC
3. Qiu, X.; Wang, N.; Wang, Z.; Wang, F.; Wang, Y. Towards high-performance zinc-based hybrid supercapacitors via macropores-based charge storage in organic electrolytes. *Angew. Chem. Int. Ed.* **2021**, *60*, 9610-7. DOI
4. Dai, H.; Zhou, R.; Zhang, Z.; Zhou, J.; Sun, G. Design of manganese dioxide for supercapacitors and zinc-ion batteries: similarities and differences. *Energy. Mater.* **2022**, *2*, 200040. DOI
5. Deng, S.; Sun, D.; Wu, C.; et al. Synthesis and electrochemical properties of MnO_2 nanorods/graphene composites for supercapacitor applications. *Electrochim. Acta.* **2013**, *111*, 707-12. DOI
6. Wu, C.; Deng, S.; Wang, H.; Sun, Y.; Liu, J.; Yan, H. Preparation of novel three-dimensional NiO/ultrathin derived graphene hybrid

for supercapacitor applications. *ACS. Appl. Mater. Interfaces.* **2014**, *6*, 1106-12. DOI

7. Ahmad, A.; Khan, S.; Javed, M. S.; et al. Improved electrochemical performance of aqueous hybrid supercapacitors using $CrCo_2O_4$ mesoporous nanowires: an innovative strategy toward sustainable energy devices. *ACS. Appl. Mater. Interfaces.* **2024**, *16*, 6920-30. DOI
8. Yan, J.; Lu, J.; Sheng, Y.; Sun, Y.; Zhang, D. Research progress in the preparation of transition metal sulfide materials and their supercapacitor performance. *Micromachines* **2024**, *15*, 849. DOI PubMed PMC
9. Wang, M.; Wang, S.; Zhao, J.; et al. Multifunctional-regions integrated with Mn-Co-Ni ternary hydroxides as self-assembled electrodes for high-performance hybrid supercapacitors. *Chem. Eng. J.* **2024**, *480*, 148206. DOI
10. Wu, S.; Yang, Y.; Sun, M.; et al. Dilute aqueous-aprotic electrolyte towards robust Zn-ion hybrid supercapacitor with high operation voltage and long lifespan. *Nano-Micro. Lett.* **2024**, *16*, 161. DOI PubMed PMC
11. Huang, T.; Gao, B.; Zhao, S.; et al. All-MXenes zinc ion hybrid micro-supercapacitor with wide voltage window based on V_2CT_x cathode and $Ti_3C_2T_x$ anode. *Nano. Energy.* **2023**, *111*, 108383. DOI
12. Yesuraj, J.; Senthamaraikannan, T. G.; Lim, D. H.; Kim, K. Construction of ternary $Zn_{0.5}Cu_{0.5}Co_2O_4$ spinel structure on nickel foam: a comprehensive theoretical and experimental study from single to ternary metal oxides for high-energy-density asymmetric supercapacitor application. *Small* **2024**, 2407608. DOI PubMed
13. Abo Kamar SM, Ibrahim AA, El-hakam SA, El-sharkawy E, Ahmed AI, Adly MS. Architecture of interconnected cubic $NiCo_2S_4$ decorated mesoporous carbon with self-doped nitrogen based-hydrogel for high performance hybrid supercapacitor. *J. Energy. Storage.* **2024**, *99*, 113384. DOI
14. Zan, G.; Li, S.; Chen, P.; Dong, K.; Wu, Q.; Wu, T. Mesoporous cubic nanocages assembled by coupled monolayers with 100% theoretical capacity and robust cycling. *ACS. Cent. Sci.* **2024**, *10*, 1283-94. DOI PubMed PMC
15. Shi, R.; Jiao, S.; Yue, Q.; Gu, G.; Zhang, K.; Zhao, Y. Challenges and advances of organic electrode materials for sustainable secondary batteries. *Exploration* **2022**, *2*, 20220066. DOI PubMed PMC
16. Gao, X.; Dong, Y.; Li, S.; Zhou, J.; Wang, L.; Wang, B. MOFs and COFs for batteries and supercapacitors. *Electrochem. Energ. Rev.* **2020**, *3*, 81-126. DOI
17. Yusran, Y.; Li, H.; Guan, X.; et al. Exfoliated mesoporous 2D covalent organic frameworks for high-rate electrochemical double-layer capacitors. *Adv. Mater.* **2020**, *32*, e1907289. DOI
18. Mahato, M.; Nam, S.; Tabassian, R.; Oh, S.; Nguyen, V. H.; Oh, I. Electronically conjugated multifunctional covalent triazine framework for unprecedented CO_2 selectivity and high-power flexible supercapacitor. *Adv. Funct. Mater.* **2022**, *32*, 2107442. DOI
19. Umezawa, S.; Douura, T.; Yoshikawa, K.; et al. Supercapacitor electrode with high charge density based on boron-doped porous carbon derived from covalent organic frameworks. *Carbon* **2021**, *184*, 418-25. DOI
20. Iqbal, R.; Majeed, M. K.; Hussain, A.; et al. Boosting the crystallinity of novel two-dimensional hexamine dipyrazino quinoxaline-based covalent organic frameworks for electrical double-layer supercapacitors. *Mater. Chem. Front.* **2023**, *7*, 2464-74. DOI
21. Kandambeth, S.; Jia, J.; Wu, H.; et al. Covalent organic frameworks as negative electrodes for high-performance asymmetric supercapacitors. *Adv. Energy. Mater.* **2020**, *10*, 2001673. DOI
22. Patra, B. C.; Bhattacharya, S. New covalent organic square lattice based on porphyrin and tetraphenyl ethylene building blocks toward high-performance supercapacitive energy storage. *Chem. Mater.* **2021**, *33*, 8512-23. DOI
23. Haldar, S.; Rase, D.; Shekhar, P.; et al. Incorporating conducting polypyrrole into a polyimide COF for carbon-free ultra-high energy supercapacitor. *Adv. Energy. Mater.* **2022**, *12*, 2200754. DOI
24. Khojastehnezhad, A.; Rhili, K.; Shehab, M. K.; et al. Rapid, mild, and catalytic synthesis of 2D and 3D COFs with promising supercapacitor applications. *ACS. Appl. Energy. Mater.* **2023**, *6*, 12216-25. DOI
25. Li, T.; Yan, X.; Zhang, W. D.; et al. A 2D donor-acceptor covalent organic framework with charge transfer for supercapacitors. *Chem. Commun.* **2020**, *56*, 14187-90. DOI
26. Li, L.; Lu, F.; Guo, H.; Yang, W. A new two-dimensional covalent organic framework with intralayer hydrogen bonding as supercapacitor electrode material. *Microporous. Mesoporous. Mater.* **2021**, *312*, 110766. DOI
27. Huang, H.; Zhao, Y.; Bai, Y.; Li, F.; Zhang, Y.; Chen, Y. Conductive metal-organic frameworks with extra metallic sites as an efficient electrocatalyst for the hydrogen evolution reaction. *Adv. Sci.* **2020**, *7*, 2000012. DOI
28. Li, X.; Liu, S.; Bai, S.; Li, Z.; Shen, J. Zeolitic-imidazolate framework derived Ni-Co layered double hydroxide hollow microspheres with enhanced pseudocapacitive properties for hybrid supercapacitors. *J. Mater. Chem. C.* **2022**, *10*, 6348-57. DOI
29. Chang, P.; Zheng, J.; Cen, Y.; et al. 3D hierarchical porous carbon from fulvic acid biomass for high energy density supercapacitor with high withstanding voltage. *J. Power. Sources.* **2022**, *533*, 231413. DOI
30. Chen, P.; Su, X.; Wang, C.; et al. Two-dimensional conjugated metal-organic frameworks with large pore apertures and high surface areas for NO_2 selective chemiresistive sensing. *Angew. Chem. Int. Ed.* **2023**, *62*, e202306224. DOI
31. Biswal, B. P.; Chandra, S.; Kandambeth, S.; Lukose, B.; Heine, T.; Banerjee, R. Mechanochemical synthesis of chemically stable isoreticular covalent organic frameworks. *J. Am. Chem. Soc.* **2013**, *135*, 5328-31. DOI PubMed
32. Li, T.; Zhang, W.; Liu, Y.; et al. A two-dimensional semiconducting covalent organic framework with nickel(II) coordination for high capacitive performance. *J. Mater. Chem. A.* **2019**, *7*, 19676-81. DOI
33. Wang, Z.; Xing, X.; Perepichka, I. F.; et al. Soluble two-dimensional donor-acceptor aza-fused aromatic frameworks and their electrochromism between the visible and near-infrared regions. *Chem. Mater.* **2022**, *34*, 4896-909. DOI
34. Zhou, R.; Huang, Y.; Li, Z.; Kang, S.; Wang, X.; Liu, S. Piperazine-based two-dimensional covalent organic framework for high

performance anodic lithium storage. *Energy. Storage. Mater.* **2021**, *40*, 124-38. DOI

35. Zhang, Z.; Zhang, Z.; Chen, C.; et al. Single-atom platinum with asymmetric coordination environment on fully conjugated covalent organic framework for efficient electrocatalysis. *Nat. Commun.* **2024**, *15*, 2556. DOI PubMed PMC
36. Shanavaz, H.; Prasanna, B.; Prashanth, M.; et al. Microwave assisted cobalt incorporated covalent organic frameworks as cathode material for asymmetric supercapacitor device. *J. Alloys. Compd.* **2024**, *970*, 172634. DOI
37. Geng, Y.; Liu, Y.; Wang, S.; Li, X.; Tang, H.; Gong, Y. Synthesis, spectroscopic characterization, crystal structure, DFT calculations, anti-cancer activities and Hirshfeld surface analysis of 2-((4-chlorophenyl)amino)-2-oxoethyl 2-ethylimidazo[1,2-a]pyridine-3-carboxylate. *J. Mol. Struct.* **2024**, *1313*, 138701. DOI
38. Li, T.; Yan, X.; Liu, Y.; et al. A 2D covalent organic framework involving strong intramolecular hydrogen bonds for advanced supercapacitors. *Polym. Chem.* **2020**, *11*, 47-52. DOI
39. Li, L.; Lu, F.; Xue, R.; et al. Ultrastable triazine-based covalent organic framework with an interlayer hydrogen bonding for supercapacitor applications. *ACS. Appl. Mater. Interfaces.* **2019**, *11*, 26355-63. DOI
40. Guo, B.; Yang, Y.; Hu, Z.; et al. Redox-active organic molecules functionalized nitrogen-doped porous carbon derived from metal-organic framework as electrode materials for supercapacitor. *Electrochim. Acta.* **2017**, *223*, 74-84. DOI
41. Park, H. W.; Roh, K. C. Recent advances in and perspectives on pseudocapacitive materials for supercapacitors-a review. *J. Power. Sources.* **2023**, *557*, 232558. DOI
42. Liu, L.; Cui, D.; Zhang, S.; et al. Triazine covalent organic framework (COF)/θ-Al_2O_3 composites for supercapacitor application. *Dalton. Trans.* **2023**, *52*, 6138-45. DOI
43. Li, T.; Feng, Q.; Wang, T.; et al. Theoretical evaluation and experimental design of nitrogen doped porous carbon from Cu-based metal-organic frameworks for lithium-ion batteries. *Surf. Interfaces.* **2022**, *30*, 101851. DOI
44. Cheng, S.; Gao, W.; Cao, Z.; Yang, Y.; Xie, E.; Fu, J. Selective center charge density enables conductive 2D metal-organic frameworks with exceptionally high pseudocapacitance and energy density for energy storage devices. *Adv. Mater.* **2022**, *34*, e2109870. DOI PubMed
45. Xu, G.; Zhu, C.; Gao, G. Recent Progress of advanced conductive metal-organic frameworks: precise synthesis, electrochemical energy storage applications, and future challenges. *Small* **2022**, *18*, e2203140. DOI PubMed
46. Xue, R.; Gou, H.; Liu, Y.; Rao, H. A layered triazinyl-COF linked by-NH-linkage and resulting N-doped microporous carbons: preparation, characterization and application for supercapacitance. *J. Porous. Mater.* **2021**, *28*, 895-903. DOI
47. Luo, X.; Zheng, H.; Lai, W.; et al. Defect engineering of carbons for energy conversion and storage applications. *Energy. Environ. Mater.* **2023**, *6*, e12402. DOI
48. Halder, A.; Karak, S.; Addicoat, M.; et al. Ultrastable imine-based covalent organic frameworks for sulfuric acid recovery: an effect of interlayer hydrogen bonding. *Angew. Chem. Int. Ed.* **2018**, *57*, 5797-802. DOI
49. Shao, Y.; El-Kady, M. F.; Sun, J.; et al. Design and mechanisms of asymmetric supercapacitors. *Chem. Rev.* **2018**, *118*, 9233-80. DOI
50. Khattak, A. M.; Ghazi, Z. A.; Liang, B.; et al. A redox-active 2D covalent organic framework with pyridine moieties capable of faradaic energy storage. *J. Mater. Chem. A.* **2016**, *4*, 16312-7. DOI
51. An, N.; Guo, Z.; Xin, J.; et al. Hierarchical porous covalent organic framework/graphene aerogel electrode for high-performance supercapacitors. *J. Mater. Chem. A.* **2021**, *9*, 16824-33. DOI
52. Bhanja, P.; Bhunia, K.; Das, S. K.; et al. A new triazine-based covalent organic framework for high-performance capacitive energy storage. *ChemSusChem* **2017**, *10*, 921-9. DOI
53. Prajapati, M.; Ravi, K. C.; Allende, S.; Jacob, M. V. Metal organic framework derived NiCo layered double hydroxide anode aggregated with biomass derived reduced graphene oxide cathode: a hybrid device configuration for supercapattery applications. *J. Energy. Storage.* **2023**, *73*, 109264. DOI
54. Li, S.; Luo, J.; Wang, J.; et al. Hybrid supercapacitors using metal-organic framework derived nickel-sulfur compounds. *J. Colloid. Interface. Sci.* **2024**, *669*, 265-74. DOI
55. Gao, Y.; Zhi, C.; Cui, P.; Zhang, K. A.; Lv, L.; Wang, Y. Halogen-functionalized triazine-based organic frameworks towards high performance supercapacitors. *Chem. Eng. J.* **2020**, *400*, 125967. DOI